

Magnetic characterization of a thin $\text{Co}_2\text{MnSi}/\text{L1}_0\text{-MnGa}$ synthetic antiferromagnetic bilayer prepared by MBE*

Shan Li(黎姗)^{1,2}, Jun Lu(鲁军)^{1,3,†}, Si-Wei Mao(毛思玮)^{1,2},
Da-Hai Wei(魏大海)^{1,2,3}, and Jian-Hua Zhao(赵建华)^{1,2,3}

¹State Key Laboratory of Superlattices and Microstructures, Institute of Semiconductors,
Chinese Academy of Sciences (CAS), Beijing 100083, China

²Center of Materials Science and Optoelectronics Engineering & CAS Center of Excellence in Topological Quantum Computation,
University of Chinese Academy of Sciences, Beijing 100190, China

³Beijing Academy of Quantum Information Science, Beijing 100193, China

(Received 14 February 2020; revised manuscript received 26 May 2020; accepted manuscript online 5 June 2020)

A synthetic antiferromagnet based on a thin antiferromagnetically coupled $\text{Co}_2\text{MnSi}/\text{MnGa}$ bilayer with Pt capping is proposed in this work. Square magnetic loops measured by anomalous Hall effect reveal that a well perpendicular magnetic anisotropy is obtained in this structure. A very large coercivity of 83 kOe ($1 \text{ Oe} = 79.5775 \text{ A}\cdot\text{m}^{-1}$) is observed near the magnetic moment compensation point of 270 K, indicating an antiferromagnetic behavior. Moreover, the anomalous Hall signal does not go to zero even at the magnetic compensation point, for which the difficulty in detecting the conventional antiferromagnets can be overcome. By changing the temperature, the polarity of the spin-orbit torque induced switching is changed around the bilayer compensation point. This kind of thin bilayer has potential applications in spin-orbit-related effects, spintronic devices, and racetrack memories.

Keywords: exchange coupling, magnetization compensation, anomalous Hall effect, molecular-beam epitaxy

PACS: 75.30.Et, 75.70.Ak, 73.50.Jt, 81.15.Hi

DOI: 10.1088/1674-1056/ab99ac

1. Introduction

Synthetic antiferromagnet (SAFM) consisting of two or more ferromagnetic layers that exhibit antiparallel magnetizations has been widely studied in recent years.^[1–5] The SAFM shares the similar advantages to innate antiferromagnets, such as the reduced stray field and the enhanced magnetic stability in micro-nano device. Because the interlayer exchange coupling in SAFM is much weaker than that of bulk antiferromagnet, the antiferromagnetic order in SAFM can be manipulated and detected more easily, which is desirable for applications in spintronic devices including ultrafast magnetic random access memory (MRAM) and high frequency oscillators.^[6] Spin-orbit torque (SOT)-induced switching was demonstrated in SAFM recently.^[7,8] And several abnormal phenomena related to SOT-induced switching were reported, such as the spin Hall angle (SHA)-like changed switching^[9] and enhanced SOT efficiency in SAFM.^[10] It was experimentally shown that large domain wall velocities were obtained in SAFM.^[11] Meanwhile, the antiferromagnetic skyrmions were studied in a perpendicular antiferromagnetic coupled system both theoretically and experimentally.^[12–23] And it was reported that the SAFM is a superior system in racetrack memory for the features of ultra-high density, ultra-high speed, and ultra-long

transmission distance due to the decreased skyrmion Hall effect.^[16] All the studies referred above imply that the SAFM is a promising material system for novel physical phenomenon study and practical application in spintronics.

Comparing with the conventional RKKY-mediated SAFM, such as $[\text{Co}/\text{Ni}]/\text{Ru}/[\text{Co}/\text{Ni}]$,^[11] $[\text{Co}/\text{Pt}]/\text{Ir}/[\text{Co}/\text{Pt}]$,^[24] $\text{CoFeB}/\text{Ru}/\text{CoFeB}$,^[7] etc., the $\text{Co}_2\text{MnSi}/\text{MnGa}$ SAFM is established by the strong antiferromagnetic interfacial exchange coupling. The MnGa is an ordered binary alloy with giant perpendicular magnetic anisotropy, and the Co_2MnSi is a half metal with high spin polarization: both have a low magnetic damping factor. So, these properties can make $\text{Co}_2\text{MnSi}/\text{MnGa}$ a more functional SAFM.^[25–28] Recently, ultrathin Co_2MnSi interlayer was induced in MnGa-based perpendicular magnetic tunneling junction (MTJ) for better device performance,^[28] $[\text{MnGa}/\text{Co}_2\text{MnSi}]_n$ superlattice was used as an MTJ reference layer for ultra-high magnetic field sensing,^[29] and the unusual anomalous Hall effect was observed in a $\text{Co}_2\text{MnSi}/\text{MnGa}/\text{Pt}$ trilayer.^[30] Nevertheless, there are few researches on its SOT effect. The antiferromagnetically coupled thin $\text{Co}_2\text{MnSi}/\text{L1}_0\text{-MnGa}$ bilayer capped with heavy metal is an ideal candidate for aforementioned novel physics study and spintronic devices application, such as

*Project supported by the National Program on Key Basic Research Project, China (Grant No. 2018YFB0407601), the Key Research Project of Frontier Science of the Chinese Academy of Sciences (Grant Nos. QYZDY-SSW-JSC015 and XDPB12), and the National Natural Science Foundation of China (Grant Nos. 11874349 and 11774339).

†Corresponding author. E-mail: lujun@semi.ac.cn

skyrmions in racetrack memory without skyrmion Hall effect and SAFM free layers in SOT-MRAM with ultrahigh magnetic stability. However, the preparation of thin $\text{Co}_2\text{MnSi}/\text{L1}_0\text{-MnGa}$ bilayer with high quality needs optimizing, and the detailed temperature and magnetic field influences on magnetic and transport properties of the thin $\text{Co}_2\text{MnSi}/\text{L1}_0\text{-MnGa}$ bilayer are still unclear, which needs further exploring.

2. Experiments

The whole structure of our sample was epitaxially grown on a GaAs (001) substrate by molecular-beam epitaxy (MBE) as shown in Fig. 1(a), in which the Co_2MnSi (0.7 nm)/ $\text{L1}_0\text{-MnGa}$ (3 nm) bilayer were grown at 250°C , while the Pt (3 nm for sample A; 5 nm for sample B) layer was deposited using e-beam evaporation at room temperature in the same

MBE growth chamber. The surface crystalline structure was monitored *in-situ* by reflection high-energy electron diffraction (RHEED). The observed streaky RHEED patterns during the growth of Co_2MnSi and MnGa indicate single crystal structure of the bilayer. The x-ray diffraction spectrum of sample A is shown in Fig. 1(c), and the fitted peaks of Pt (002) and MnGa (002) are shown in Fig. 1(d). The reference sample (sample R: Co_2MnSi (20 nm)/ $\text{L1}_0\text{-MnGa}$ (28 nm))^[28] was also grown by MBE. The magnetization measurements were carried out by using the superconducting quantum interference device (SQUID) magnetometer. The samples were then patterned into Hall bars with $10\ \mu\text{m}$ in width and $120\ \mu\text{m}$ in length by ultraviolet lithography and dry etching, and the gold contact electrodes were deposited by thermal evaporation as shown in Fig. 1(b). The anomalous Hall resistance was measured by the physical property measurement system (PPMS).

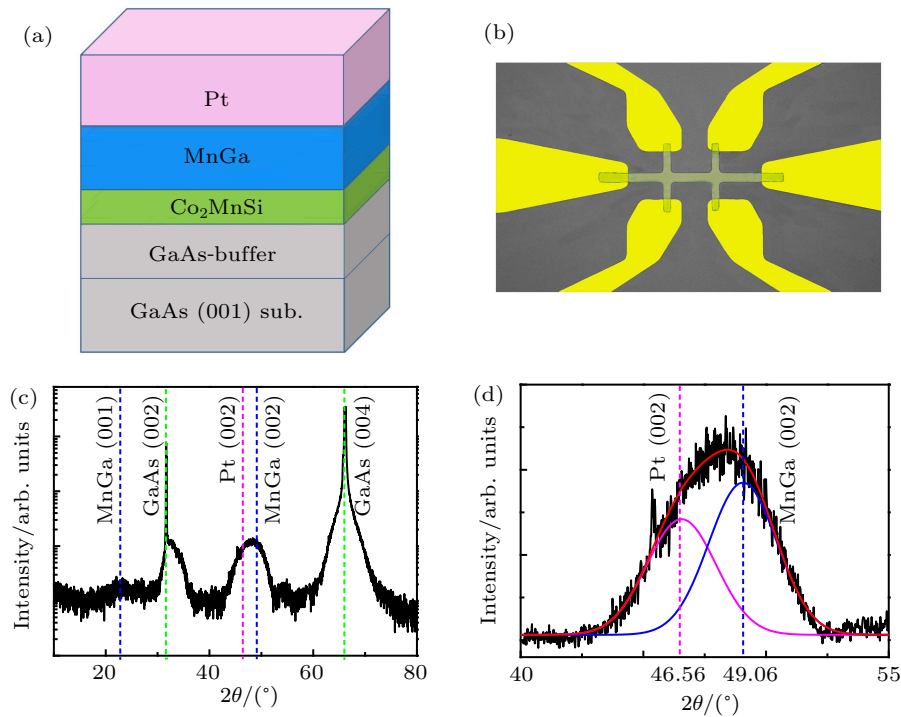


Fig. 1. (a) Schematic diagram of sample structure, (b) microscope photograph of Hall bar device ($120\ \mu\text{m} \times 10\ \mu\text{m}$), (c) x-ray diffraction spectrum of the Co_2MnSi (0.7 nm)/ $\text{L1}_0\text{-MnGa}$ (3 nm)/Pt (3 nm) structure, and (d) fitted peaks of Pt (002) and MnGa (002) of the Co_2MnSi (0.7 nm)/ $\text{L1}_0\text{-MnGa}$ (3 nm)/Pt (3 nm) structure, with black, red, pink, and blue curves representing the experimental data, fitted sum of peaks, fitted Pt (002) peak, and fitted MnGa (002) peak, respectively.

3. Results and discussion

Considering the small net saturation magnetization in SAFM and the poor signal-to-noise ratio in magnetic measurement, the anomalous Hall effect (AHE) is used to characterize the magnetic properties of the SAFM. For a bilayer, the total AHE voltage is a superposition of two parallel signals, which are determined by both of magnetization and the AHE coefficient in each layer, so a nonzero AHE voltage is expected even at the magnetic moment compensation point.

The anomalous Hall resistance (R_{AH}) and the magnetic hysteresis loops of sample R are shown in Figs. 2(a) and 2(b), respectively. The magnetic field-induced magnetization rotation and switching of the Co_2MnSi layer are independent of the MnGa layer in the bilayer due to their large thickness. The consistent trends of the AHE and the magnetic hysteresis loops indicate that the AHE coefficient of Co_2MnSi and MnGa are both positive. And the signal ratio of $\text{Co}_2\text{MnSi}/\text{MnGa}$ is much larger in the AHE loop than in the magnetic hysteresis loop, which indicate that Co_2MnSi and MnGa have different AHE

coefficients. From Fig. 2(b), the saturated magnetization of Co_2MnSi and MnGa are calculated to be 640 emu/cm^3 and 96 emu/cm^3 , respectively. And the interfacial antiferromagnetic coupling constant is about -5 erg/cm^2 ($1 \text{ erg} = 10^{-7} \text{ J}$) as reported in our previous work.^[28] Therefore, a compensated SAFM bilayer can be designed if the thickness ratio of Co_2MnSi to MnGa is much reduced to about 1:6.7, and the magnetic and transport properties can be characterized by AHE near the magnetic compensation point. To achieve perpendicular thin SAFM, considering the exchange length of MnGa and the critical thickness of forming continuous film of Co_2MnSi ,^[28,29] the Co_2MnSi (0.7 nm)/ $\text{Ll}_0\text{-MnGa}$ (3 nm) bilayer is selected.

The AHE loops of sample A at different temperatures are shown in Fig. 2(c). The coercivity (H_c) of the structure is very large, and a polarity reverse of R_{AH} is obtained in a range from 250 K to 200 K. Compared with the monotonical change of H_c with temperature of MnGa single layer,^[31] the change of the H_c with temperature is non-monotonical in the Co_2MnSi

(0.7 nm)/ $\text{Ll}_0\text{-MnGa}$ (3 nm) bilayer, and a peak of H_c (about 83 kOe) is obtained at 250 K as shown in Fig. 2(d). In addition, because of the distinct temperature dependence of magnetization between MnGa and Co_2MnSi , the completely compensated antiferromagnetic state will be achieved by changing temperature. As shown in Fig. 2(d), the out-of-plane remnant magnetization of sample A passes through zero point with temperature decreasing, and the compensation temperature is around 270 K. This behavior is much different from that in single MnGa layer, which behaves like conventional perpendicular ferromagnet where the residual magnetization decreases with temperature increasing up to the Curie point.^[32] Near the compensation point, the Co_2MnSi (0.7 nm)/ $\text{Ll}_0\text{-MnGa}$ (3 nm) bilayer is not sensitive to the external magnetic field, and a large H_c and a small saturation magnetization are expected, which is consistent with the results of Fig. 2(d). As a result, the thin Co_2MnSi (0.7 nm)/ $\text{Ll}_0\text{-MnGa}$ (3 nm) bilayer behaves like an antiferromagnet.

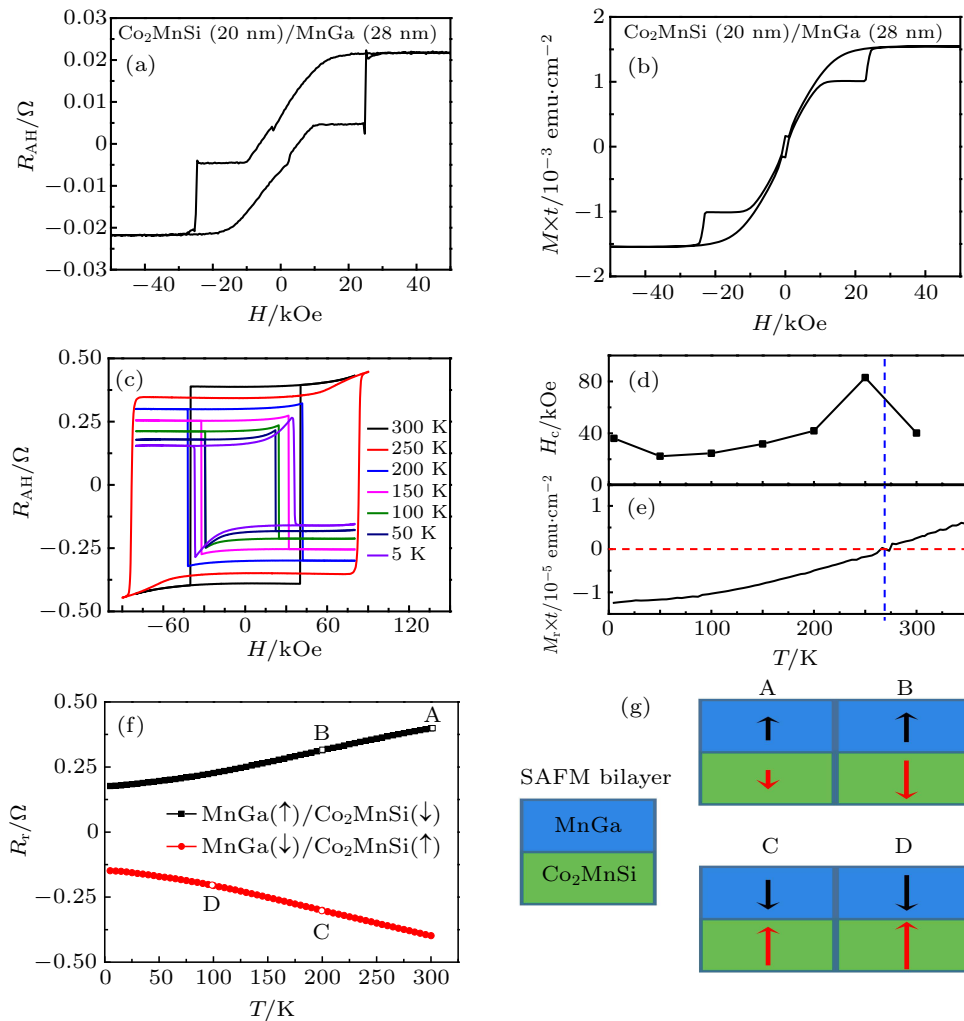


Fig. 2. (a) R_{AH} loop and (b) out-of-plane magnetic hysteresis loop at room temperature of sample R. (c) R_{AH} loops of sample A at different temperatures. (d) Plots of temperature-dependent coercivity and out-of-plane remnant magnetization of sample A. (e) Plot of temperature-dependent out-of-plane remnant magnetization of sample A. (f) Remnant Hall resistance varying with temperature of sample A, showing opposite magnetic configurations in the process of temperature changing. (g) Schematic diagrams of the magnetic moment states at points A, B, C and D of (e) with “↑” and “↓” representing the magnetic moments parallel and antiparallel to the positive direction separately.

An obvious R_{AH} polarity transition from 250 K to 200 K of the SAFM is observed in Fig. 2(c). There are two possible reasons: one is the polarity change of AHE with temperature sweeping, which was reported in SrRuO₃^[33,34] and Mn₂CoAl single layer;^[35] the other is the magnetic configuration transition of the bilayer, similar to the change of AHE polarity in CoTb^[36,37] with the Co composition. Further studies of the SAFM by manipulating the temperature and magnetic field are demonstrated. As shown in Fig. 2(e), the remnant R_{AH} of the bilayer after technical magnetization does not possess compensated point in a temperature range from 5 K to 300 K, considering the fact that the magnetic configuration of the bilayer cannot be changed with the temperature sweeping, thus, the polarity change of R_{AH} loops in a temperature range of 200 K to 250 K arises from the different magnetic configurations of the SAFM bilayer. Combining with Fig. 2(c), several specific points are selected to analyze the magnetic configuration. Points A (C) and B (D) have the same magnetic configuration, but the magnetic configuration B can be obtained only by sweeping magnetic field from a negative value of -5 T to zero, for which the sweeping direction is opposite to that for the magnetic configuration C, as shown in Fig. 2(f). That means that B and C have opposite magnetic configurations, which are mainly dependent on the Zeeman energy of the net magnetic moment of the bilayer. And the polarity of R_{AH} is expected to be positive (negative) at 300 K (200 K) due to the much larger AHE contribution from MnGa layer on both sides of the compensation point.

In order to further understand the magnetic dynamic properties of the thin Co₂MnSi/L1₀-MnGa SAFM, we conduct a preliminary SOT-induced switching test. To achieve a more easily detectable SOT-induced switching, sample B (Co₂MnSi (0.7 nm)/L1₀-MnGa (3 nm)/Pt (5 nm)) is prepared, in which the SAFM is covered with thicker Pt. As shown in Figs. 3(a) and 3(b), the polarities of R_{AH} are reversed between 280 K and 240 K. According to the previous analysis, the polarity reversal of R_{AH} is caused by opposite magnetic configuration, which is determined by Zeeman energy of the net magnetic moment of SAFM. Along the positive direction of the current, an external magnetic field of 2 T is applied to the system, and further studies of the SOT-induced switching are shown in Figs. 3(c) and 3(d). Considering the fact that the resistivity of L1₀-MnGa and Pt are approximately 100 $\mu\Omega\cdot\text{cm}$ ^[31] and 10 $\mu\Omega\cdot\text{cm}$ and the resistivity of Co₂MnSi is close to that of Pt,^[38,39] the critical current density is about $4.9\times 10^7\text{A}/\text{cm}^2$ at 280 K and $5.8\times 10^7\text{A}/\text{cm}^2$ at 240 K. The chirality of SOT-induced switching loops are consistent with the AHE loops, which is similar to the reported phenomenon that the chirality of SOT-induced switching loops are opposite on both sides

of the component compensation point of ferrimagnets.^[36,40] Moreover, it is demonstrated that in addition to controlling the direction of the external magnetic field or electrical current, changing the external temperature is also a method to invert the polarity of SOT-induced switching loop in the SAFM.

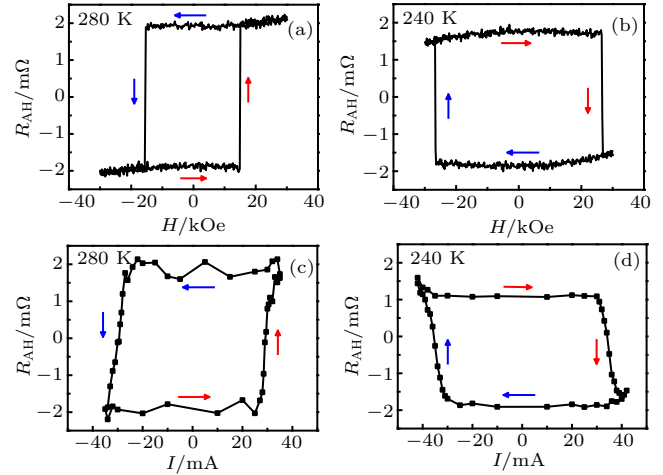


Fig. 3. R_{AH} loop at (a) 280 K and (b) 240 K and SOT-induced switching loop at (c) 280 K and (d) 240 K, of sample B (Co₂MnSi (0.7 nm)/L1₀-MnGa (3 nm)/Pt (5 nm)).

4. Conclusions

In this work, the perpendicular thin Co₂MnSi/MnGa SAFM bilayer is epitaxially grown on a GaAs (001) substrate. The magnetic compensation point is achieved near 270 K, and an ultra-large coercivity of 83 kOe is observed around this point. Moreover, the magnetic configuration in this bilayer during technical magnetization is mainly determined by the Zeeman energy of the net magnetic moment, which is demonstrated in detail by the temperature dependence of the remnant Hall resistance at zero magnetic field. The SOT-induced switching loops also have opposite polarities at the temperatures lower and higher than the compensated temperature in Co₂MnSi/MnGa/Pt structure. Our work reveals that the thin Co₂MnSi/MnGa bilayer behaves like an antiferromagnet, and may promote its application in spintronic devices as an SAFM.

References

- [1] Ackermann M S and Emori S 2018 *J. Appl. Phys.* **124** 223901
- [2] Chen R Y, Zhang R Q, Liao L Y, Chen X Z, Zhou Y J, Gu Y D, Saleem M S, Zhou X F, Pan F and Song C 2019 *Appl. Phys. Lett.* **115** 132403
- [3] Fernandez-Pacheco A, Vedmedenko E, Ummelen F, Mansell R, Petit D and Cowburn R P 2019 *Nat. Mater.* **18** 679
- [4] Han D S, Lee K, Hanke J P, Mokrousov Y, Kim K W, Yoo W, van Hees Y L W, Kim T W, Lavrijsen R, You C Y, Swagten H J M, Jung M H and Klauui M 2019 *Nat. Mater.* **18** 703
- [5] Li Y, Jin X, Pan P, Tan F N, Lew W S and Ma F 2018 *Chin. Phys. B* **27** 127502
- [6] Duine R A, Lee K J, Parkin S S P and Stiles M D 2018 *Nat. Phys.* **14** 217
- [7] Shi G Y, Wan C H, Chang Y S, Li F, Zhou X J, Zhang P X, Cai J W, Han X F, Pan F and Song C 2017 *Phys. Rev. B* **95** 104435

- [8] Moriyama T, Zhou W, Seki T, Takanashi K and Ono T 2018 *Phys. Rev. Lett.* **121** 167202
- [9] Bi C, Almasi H, Price K, Newhouse-Illige T, Xu M, Allen S R, Fan X and Wang W 2017 *Phys. Rev. B* **95** 104434
- [10] Zhang P X, Liao L Y, Shi G Y, Zhang R Q, Wu H Q, Wang Y Y, Pan F and Song C 2018 *Phys. Rev. B* **97** 214403
- [11] Yang S H, Ryu K S and Parkin S 2015 *Nat. Nanotechnol.* **10** 221
- [12] Barker J and Tretiakov O A 2016 *Phys. Rev. Lett.* **116** 147203
- [13] Jin C, Song C, Wang J and Liu Q 2016 *Appl. Phys. Lett.* **109** 182404
- [14] Lee J C T, Chess J J, Montoya S A, Shi X, Tamura N, Mishra S K, Fischer P, McMorran B J, Sinha S K, Fullerton E E, Kevan S D and Roy S 2016 *Appl. Phys. Lett.* **109** 022402
- [15] Zhang X, Zhou Y and Ezawa M 2016 *Sci. Rep.* **6** 24795
- [16] Zhang X, Zhou Y and Ezawa M 2016 *Nat. Commun.* **7** 10293
- [17] Kim S K, Lee K J and Tserkovnyak Y 2017 *Phys. Rev. B* **95** 140404(R)
- [18] Xia H, Jin C, Song C, Wang J, Wang J and Liu Q 2017 *J. Phys. D: Appl. Phys.* **50** 505005
- [19] Akosa C A, Tretiakov O A, Tatara G and Manchon A 2018 *Phys. Rev. Lett.* **121** 097204
- [20] Caretta L, Mann M, Buttner F, Ueda K, Pfau B, Gunther C M, Hessing P, Churikova A, Klose C, Schneider M, Engel D, Marcus C, Bono D, Bagschik K, Eisebitt S and Beach G S D 2018 *Nat. Nanotechnol.* **13** 1154
- [21] Xing L, Hua D and Wang W 2018 *J. Appl. Phys.* **124** 123904
- [22] Hirata Y, Kim D H, Kim S K, Lee D K, Oh S H, Kim D Y, Nishimura T, Okuno T, Futakawa Y, Yoshikawa H, Tsukamoto A, Tserkovnyak Y, Shiota Y, Moriyama T, Choe S B, Lee K J and Ono T 2019 *Nat. Nanotechnol.* **14** 232
- [23] Khoshlahni R, Qaiumzadeh A, Bergman A and Brataas A 2019 *Phys. Rev. B* **99** 054423
- [24] Fache T, Tarazona H S, Liu J, L'vova G, Applegate M J, Rojas-Sanchez J C, Petit-Watelot S, Landauro C V, Quispe-Marcatoma J, Morgunov R, Barnes C H W and Mangin S 2018 *Phys. Rev. B* **98** 064410
- [25] Ranjbar R, Suzuki K Z, Sugihara A, Ando Y, Miyazaki T and Mizukami S 2017 *J. Magn. Magn. Mater.* **433** 195
- [26] Ranjbar R, Suzuki K, Sugihara A, Miyazaki T, Ando Y and Mizukami S 2015 *Materials (Basel)* **8** 6531
- [27] Ma Q L, Mizukami S, Kubota T, Zhang X M, Ando Y and Miyazaki T 2014 *Phys. Rev. Lett.* **112** 157202
- [28] Mao S W, Lu J, Zhao X P, Wang X L, Wei D H, Liu J, Xia J B and Zhao J H 2017 *Sci. Rep.* **7** 43064
- [29] Lu J, Mao S W, Zhao X P, Wang X L, Liu J, Xia J B, Xiong P and Zhao J H 2017 *Sci. Rep.* **7** 16990
- [30] Li S, Lu J, Wen L J, Pan D, Wang H L, Wei D H and Zhao J H 2020 *Chin. Phys. Lett.* **37** 077303
- [31] Zhu L J, Pan D and Zhao J H 2014 *Phys. Rev. B* **89** 220406(R)
- [32] Zhu L J, Pan D, Nie S H, Lu J and Zhao J H 2013 *Appl. Phys. Lett.* **102** 132403
- [33] Matsuno J, Ogawa N, Yasuda K, Kagawa F, Koshibae W, Nagaosa N, Tokura Y and Kawasaki M 2016 *Sci. Adv.* **2** e1600304
- [34] Kan D, Moriyama T, Kobayashi K and Shimakawa Y 2018 *Phys. Rev. B* **98** 18048(R)
- [35] Ludbrook B M, Dubuis G, Puichaud A H, Ruck B J and Granville S 2017 *Sci. Rep.* **7** 13620
- [36] Finley J and Liu L 2016 *Phys. Rev. Appl.* **6** 054001
- [37] Siddiqui S A, Han J, Finley J T, Ross C A and Liu L 2018 *Phys. Rev. Lett.* **121** 057701
- [38] Wang W H, Ren X B, Wu G H, Przybylski M, Barthel J, and Kirschner J 2005 *IEEE Trans. Magn.* **41** 2805
- [39] Wang W H, Ren X B, Wu G H, Przybylski M, Barthel J, and Kirschner J 2017 *Phys. Rev. Lett.* **118** 167201
- [40] Mishra R, Yu J, Qiu X, Motapothula M, Venkatesan T and Yang H 2017 *Phys. Rev. Lett.* **118** 167201